

Genuine and Robust Magnetoelectric Coupling Effect in van der Waals Multiferroic Tunnel Junctions

Zhi Yan,^{1,2,*} Xujin Zhang,¹ Jianhua Xiao,¹ Cheng Fang,¹ and Xiaohong Xu^{1,2,†}

¹*School of Chemistry and Materials Science & Key Laboratory of Magnetic Molecules and Magnetic Information Materials of Ministry of Education, Shanxi Normal University, Taiyuan 030031, China*

²*Research Institute of Materials Science & Shanxi Key Laboratory of Advanced Magnetic Materials and Devices, Shanxi Normal University, Taiyuan 030031, China*

(Dated: January 7, 2025)

Van der Waals multiferroic tunnel junctions (vdW-MFTJs) are promising candidates for data storage devices due to their tunable thickness and capability to exhibit multiple nonvolatile resistance states. However, existing vdW-MFTJs utilize ferroelectricity and ferromagnetism independently, failing to achieve true magnetoelectric coupling, which leads to unnecessary energy dissipation. Here, we propose an innovative vdW-MFTJ design based on a CrBr₃/MnPS₃/CrBr₃ vertical heterostructure, enabling genuine magnetoelectric coupling without relying on atomic migration induced by inversion symmetry breaking for ferroelectric polarization reversal. Using first-principles calculations, we investigate the spin-polarized quantum transport properties of the proposed structure. By integrating asymmetric PtTe₂/alkali-metal (Li/Na/K)-doped/intercalated CrBr₃ electrodes, the device demonstrates exceptional performance, with a maximum tunneling magnetoresistance (TMR) exceeding $8.1 \times 10^5\%$ and tunneling electroresistance (TER) reaching 2499%, while the spin-filtering channels can be flexibly controlled by the magnetization direction of the magnetic free layer, achieving perfect spin-filtering over a broad bias voltage range. Applying an external bias voltage further enhances these metrics, increasing TMR to $3.6 \times 10^7\%$ and TER to 9990%. Notably, a pronounced negative differential resistance (NDR) effect is observed, yielding an unprecedented peak-to-valley ratio (PVR) of $9.55 \times 10^9\%$, representing the highest value reported for vertical tunnel junctions. These extraordinary characteristics highlight the potential of vdW-MFTJs for ultra-efficient electronic switching, a key feature for next-generation spintronic devices. Our findings provide a solid theoretical foundation for designing and developing high-performance magnetic storage and logic technologies.

Introduction.—The advancement of memory and logic technologies increasingly hinges on multifunctional devices capable of integrating diverse physical properties [1, 2]. Among these, van der Waals (vdW) heterostructures—assembled from atomically thin layers with weak interlayer coupling—have emerged as prime candidates for next-generation electronics due to their unparalleled tunability and intrinsic low-dimensional nature [3–8]. In particular, vdW multiferroic tunnel junctions (vdW-MFTJs) have garnered attention for data storage applications, owing to their ability to exhibit multiple nonvolatile resistance states driven by the coexistence of ferroelectricity and ferromagnetism. Their adjustable thickness and interfacial properties offer a versatile platform for engineering quantum transport phenomena [9, 10]. Despite extensive studies [11–20], most existing vdW-MFTJs treat ferroelectricity and ferromagnetism as independent effects, mechanically combining them without achieving direct magnetoelectric coupling. This limitation results in suboptimal device performance and unnecessary energy dissipation, underscoring the need for innovative designs that achieve genuine magnetoelectric coupling.

Overcoming the intrinsic decoupling between spin and charge degrees of freedom to realize genuine magnetoelectric coupling remains a significant challenge [21–23]. Recent advances in two-dimensional (2D) multiferroic systems have explored two primary classes of coupling mechanisms [24–26]. The first involves type-I multiferroics, such as FeI₂/In₂Se₃ [27], CrI₃/Sc₂Co₂ [28], and charged CrBr₃ [29], while the second focuses on type-II multiferroics, including

Hf₂VC₂F₂ [30], VOI₂ [31], and MnCl₂ [32]. However, these systems face critical limitations: weak magnetoelectric coupling and the confinement of ferroelectric polarization to in-plane directions, which is less practical for device integration. Recently, a CrBr₃/MnPS₃/CrBr₃ heterostructure was proposed [33], demonstrating spin-induced out-of-plane ferroelectricity and robust magnetoelectric coupling. This heterostructure shows promise as a building block for vdW-MFTJs. However, achieving enhanced spin filtering, tunable resistance ratios, and nontrivial quantum effects in vdW-MFTJs remains a formidable challenge.

In this Letter, we present a novel vdW-MFTJ design based on a CrBr₃/MnPS₃/CrBr₃ vertical heterostructure, offering genuine magnetoelectric coupling without relying on conventional atomic migration induced by inversion symmetry breaking for polarization reversal. Employing first-principles calculations, we investigated its spin-polarized quantum transport properties and demonstrated remarkable performance enhancements through the integration of asymmetric PtTe₂/alkali-metal (Li/Na/K)-doped/intercalated CrBr₃ electrodes. The proposed design exhibits exceptional tunneling magnetoresistance (TMR) and tunneling electroresistance (TER), reaching $8.1 \times 10^5\%$ and 2499%, respectively, along with perfect spin-filtering effects over a broad bias voltage range. Furthermore, applying an external bias voltage amplifies these metrics to unprecedented levels, with TMR and TER increasing to $3.6 \times 10^7\%$ and 9990%, respectively. Notably, the device displays a pronounced negative differential resistance (NDR) effect, characterized by a peak-to-valley ra-

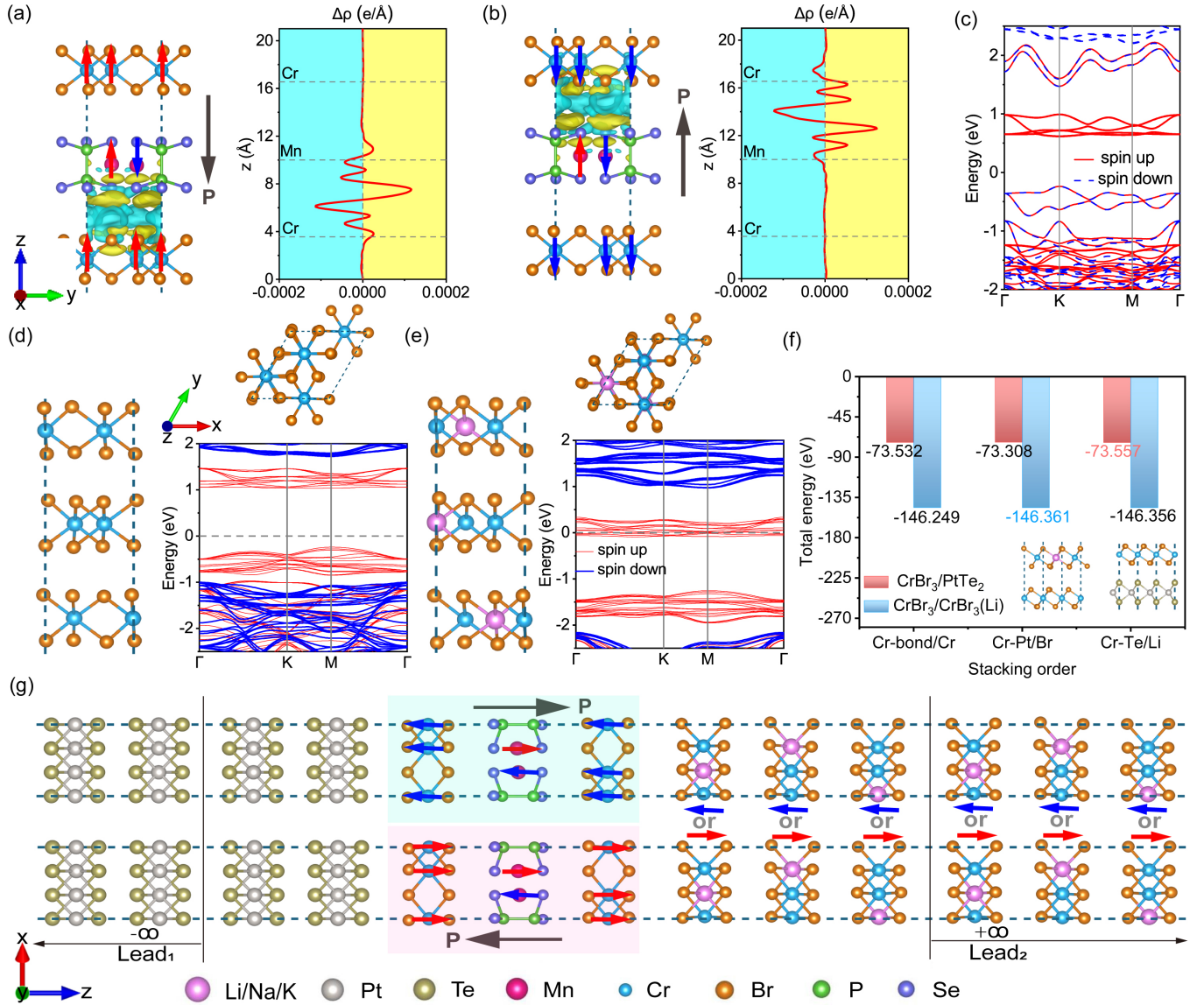


FIG. 1. (a) and (b) Side views of the CrBr₃/MnPSe₃/CrBr₃ heterostructure showing the differential charge density between the out-of-plane ferroelectric and non-polarized states, with plane-averaged plots. Electron accumulation and depletion are indicated by yellow and cyan isosurfaces, set at $1.65 \times 10^{-5} e/\text{Bohr}^3$. (c) Electronic band structure of the CrBr₃/MnPSe₃/CrBr₃ heterostructure. (d) and (e) Side and top views of the bulk CrBr₃ crystal, the Li-intercalated CrBr₃ structure, and their corresponding band structures. (f) Total energy at the CrBr₃/PtTe₂ and CrBr₃/BrCr₃(Li) interfaces for various stacking sequences, with insets showing the optimal stacking configurations. (g) Schematic diagram of the PtTe₂/CrBr₃/MnPSe₃/CrBr₃/CrBr₃(Li/Na/K) vdW-MFTJs device model, periodic in the xy -plane, with current flowing along the z -direction.

tio (PVR) as high as $9.55 \times 10^9\%$, the largest reported in vertical tunnel junctions. These extraordinary properties underscore the transformative potential of vdW-MFTJs for ultra-efficient electronic switching, laying a robust theoretical foundation for next-generation spintronic devices and advancing high-performance magnetic storage and logic technologies.

The establishment of vdW-MFTJs models.—The ferroelectricity observed in vdW-MFTJs is primarily driven by the intrinsic ferroelectric properties of the materials. Switching the ferroelectric polarization direction results in structural

changes, such as sliding [11] or atomic migration [14, 34], which breaks the inversion symmetry. This process typically requires mechanical energy or an external electric field, making it unsuitable for low-power devices. A recent study [33] proposed that spin-driven ferroelectricity, which preserves structural inversion symmetry, can be observed in the vertically stacked CrBr₃/MnPSe₃/CrBr₃ heterostructure. This structure, therefore, holds promise as a core component for vdW-MFTJs, enabling low-power, all-magnetic control of ferroelectric behavior. Figures 1(a) and 1(b) illustrate in detail

TABLE I. Calculated the spin-resolved electron transmission T_{\uparrow} and T_{\downarrow} , TMR, TER, and SIE of PtTe₂/CrBr₃/MnPSe₃/CrBr₃/CrBr₃(Li/Na/K) vdW-MFTJs at equilibrium state.

Dopant Atom	Polarization and Ratio	PC state (M $\uparrow\uparrow$)				APC state (M $\uparrow\downarrow$)				TMR
		T_{\uparrow}	T_{\downarrow}	$T_{\text{tot}} = T_{\uparrow} + T_{\downarrow}$	SIE	T_{\uparrow}	T_{\downarrow}	$T_{\text{tot}} = T_{\uparrow} + T_{\downarrow}$	SIE	
Li	P \rightarrow	9.75×10^{-7}	3.22×10^{-24}	9.75×10^{-7}	100 %	8.45×10^{-24}	7.33×10^{-10}	7.33×10^{-10}	100 %	132915%
	P \leftarrow	3.29×10^{-24}	2.29×10^{-7}	2.29×10^{-7}	100 %	2.82×10^{-11}	7.86×10^{-24}	2.82×10^{-11}	100 %	811957%
	TER	326%				2499%				
Na	P \rightarrow	3.26×10^{-10}	4.40×10^{-24}	3.26×10^{-10}	100 %	8.25×10^{-24}	2.33×10^{-13}	2.33×10^{-13}	100 %	139814%
	P \leftarrow	4.49×10^{-24}	1.71×10^{-10}	1.71×10^{-10}	100 %	8.49×10^{-14}	8.91×10^{-24}	8.49×10^{-14}	100 %	201313%
	TER	91%				174%				
K	P \rightarrow	1.58×10^{-10}	4.10×10^{-24}	1.58×10^{-10}	100 %	6.15×10^{-24}	1.61×10^{-13}	1.61×10^{-13}	100 %	98037%
	P \leftarrow	4.20×10^{-24}	1.52×10^{-10}	1.52×10^{-10}	100 %	4.61×10^{-14}	8.54×10^{-23}	4.61×10^{-14}	100 %	329618%
	TER	3.9%				249%				

the correlation between the magnetic ordering of the magnetic atoms and the out-of-plane ferroelectricity in this heterostructure. The ferroelectric polarization strength, calculated via the Berry phase method [35], is 0.33 pC/m. When the CrBr₃ layers on both sides of MnPSe₃ adopt antiferromagnetic ordering, the system exhibits no ferroelectricity, as the geometric and magnetic ordering maintain inversion symmetry. The differential charge density and the planar-averaged plot between the ferroelectric and non-ferroelectric states further confirm the magnetoelectric coupling effect [see Figs. 1(a) and 1(b)]. Figure. 1(c) shows that the CrBr₃/MnPSe₃/CrBr₃ heterojunction exhibits magnetic semiconductor behavior. The spin-down bands display half-metallic characteristics in the energy range of approximately 0.5 eV to 1.0 eV, making this structure an ideal candidate for use as both the barrier and magnetic layers in vdW-MFTJs.

The choice of electrodes is crucial for the device performance. In our previous work [36], we proposed alkali metal (Li/Na/K) doping as a strategy to induce a semiconductor-to-half-metal transition in CrCl₃. As shown in Figs. 1(d) and 1(e), Li doping shifts the Fermi level of bulk CrBr₃ into the spin-down band region, achieving half-metallicity. To ensure experimental feasibility, we also employed a Li intercalation approach, utilizing the well-established ionic intercalation technique [37] to introduce Li into the vdW gaps of multilayer CrBr₃, which similarly results in half-metallic behavior [Fig. S1(b) in the Supplemental Material [38]]. Thus, alkali metal (Li/Na/K)-doped or intercalated CrBr₃ can serve as an electrode. For the asymmetric electrodes required in ferroelectric tunnel junctions, we chose vdW PtTe₂ with metallic properties [see the band structure in Fig.S1(a) in the Supplemental Material [38]] as another electrode. The optimized in-plane lattice constant for PtTe₂ (3.89 Å) and CrBr₃ (6.42 Å) correspond to a minimal supercell lattice mismatch of 4.7% for a $\sqrt{3} \times \sqrt{3} @ 1 \times 1$ configuration. We also calculated the stacking configurations for the CrBr₃/PtTe₂ and CrBr₃/CrBr₃(Li) heterojunction interfaces [Fig. 1(f)], finding that the energetically

favorable stackings are Cr-Te and Cr-Br, respectively. Based on these results, we constructed a fully vdW heterostructure device, PtTe₂/CrBr₃/MnPSe₃/CrBr₃/CrBr₃(Li/Na/K), as vdW-MFTJs [see Fig 1(g) and Fig.S1(c) in the Supplemental Material [38]].

Electronic and transport properties at equilibrium.—The mechanism of traditional MFTJs relies on external magnetic or electric fields to switch the polarization direction of the magnetic free layer or electrostatic barrier, resulting in four non-volatile resistance states: the magnetic ordering-dependent parallel (PC) and antiparallel (APC) configurations, and the ferroelectric polarization-dependent P \rightarrow and P \leftarrow states. In contrast, due to the unique magnetoelectric coupling in the CrBr₃/MnPSe₃/CrBr₃ heterostructure, the control of these four resistance states can be achieved solely by an external magnetic field, enabling low-power operation of our MFTJs. We first investigated the electronic transport properties of PtTe₂/CrBr₃/MnPSe₃/CrBr₃/CrBr₃(Li/Na/K) vdW-MFTJs at equilibrium. As summarized in Table I, Li/Na/K doping induces significant TMR and TER effects at equilibrium, with maximum values of $8.1 \times 10^5\%$ and 2499%, respectively. Furthermore, all four non-volatile resistance states exhibit perfect spin filtering effects, and the direction of the magnetic free layer can flexibly switch the spin channels. The experimentally feasible Li intercalation strategy for CrBr₃ is detailed in Table SI of the Supplemental Material [38]. Despite a one-order-of-magnitude reduction in TMR/TER, Li intercalation preserves the perfect spin filtering effect, with the TMR/TER still remaining substantial. Therefore, these vdW-MFTJs exhibit giant TMR/TER and perfect spin filtering effects with tunable spin channels, showcasing their significant potential for spintronic applications.

The electronic properties of the central scattering region in MFTJs provide insight into the physical mechanisms underlying the non-volatile resistive states. We analyze the Li-doped MFTJs as representatives. As depicted in Fig. 2, regardless of the magnetic and ferroelectric configurations, the Fermi level

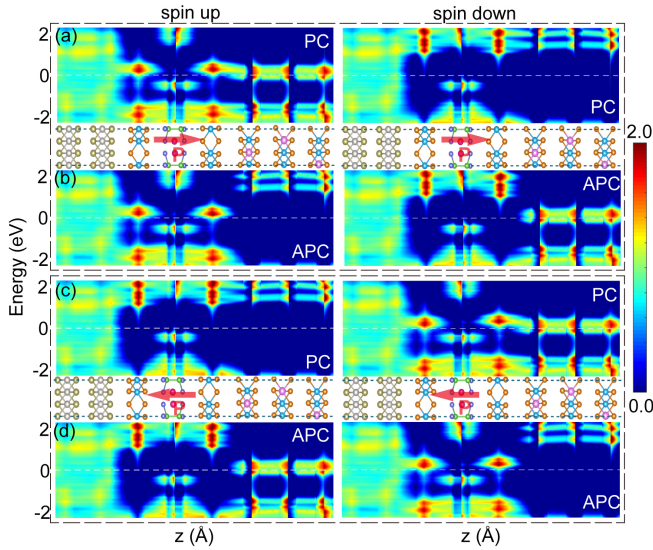


FIG. 2. Spin-resolved projected density of states (PDOS) and the corresponding crystal structure of the central scattering region along the transport direction (z -axis) of the equilibrium state for $\text{PtTe}_2/\text{CrBr}_3/\text{MnPSe}_3/\text{CrBr}_3/\text{CrBr}_3(\text{Li})$ MFTJ. Panels (a) and (b) correspond to the polarization state $P \rightarrow$, while panels (c) and (d) correspond to the polarization state $P \leftarrow$. The Fermi level is indicated by a white dashed line.

at the MnPSe_3 position lies within a non-electronic state region, indicating that electron transport occurs via tunneling. Figure 2 also demonstrates the typical TMR effect. Taking the $P \rightarrow$ state as an example, the spin-up density of states (DOS) in Fig. 2(a) shows that the $\text{CrBr}_3/\text{MnPSe}_3/\text{CrBr}_3$ heterostructure as a whole and the Li-doped CrBr_3 magnetic free layer can be regarded as majority states due to the significant DOS accumulation near the Fermi level. In contrast, for the spin-down channel, the absence of DOS at the Fermi level for both cases indicates their minority states. In the APC state [Fig. 2(b)], spin-up (spin-down) electrons injected from the left electrode pass through the majority (minority) states of the $\text{CrBr}_3/\text{MnPSe}_3/\text{CrBr}_3$ structure and exit through the minority (majority) states of the Li-doped CrBr_3 magnetic electrode. This opposite alignment of electronic states impedes electron transmission, leading to a high-resistance state. In the PC state [Fig. 2(a)], the spin-up and spin-down states correspond to majority-to-majority and minority-to-minority transitions, respectively, dictating the low- and high-resistance transport behaviors and yielding a perfect spin-filtering effect, as summarized in Table I.

To comprehensively analyze the effects of ferroelectric polarization and magnetization alignment on electron transmission, we calculated the k_{\parallel} -resolved transmission coefficients at the Fermi level within the 2D Brillouin zone (2D-BZ). Figures 3(a) and 3(b) show that, in the $P \rightarrow$ state, hotspots appear predominantly in the spin-up/spin-down channels of the PC/APC states, with fewer in the spin-down/up channels, indicating a clear spin-filtering effect and magnetization-controlled spin channels. Comparing Figs. 3(a) and 3(b),

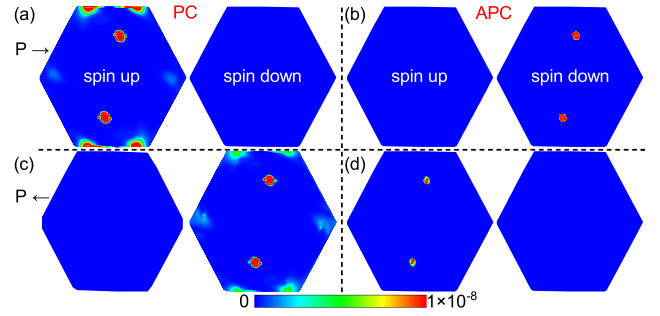


FIG. 3. The k_{\parallel} -resolved transmission coefficients of $\text{PtTe}_2/\text{CrBr}_3/\text{MnPSe}_3/\text{CrBr}_3/\text{CrBr}_3(\text{Li})$ MFTJs in the 2D Brillouin zone at the Fermi level for the $P \rightarrow/P \leftarrow$ and $PC(M\uparrow\uparrow)/APC(M\uparrow\downarrow)$ states.

the $PC(M\uparrow\uparrow)$ state exhibits significantly more hotspots in the spin-conducting channel than the $APC(M\uparrow\downarrow)$ state, suggesting a strong TMR effect. A similar trend is observed in the $P \leftarrow$ state, with reversed spin-filtering channels. A large TER effect is apparent when comparing the hotspot distributions between the $P \rightarrow$ and $P \leftarrow$ states: the distribution in Fig. 3(a) is larger than in Fig. 3(c), and in Fig. 3(b) it is larger than in Fig. 3(d). Figures S2 and S3 in the Supplemental Material [38] present the PDOS and electronic transmission spectra in the 2D-BZ distribution for Na- and K-doped as well as Li-intercalated electrodes. The analysis above is directly applicable to these cases and will not be repeated here.

Transport properties at nonequilibrium.—In this section, we calculate the bias voltage-dependent (ranging from -1.2 to 1.2 V) spin-polarized current, spin injection efficiency (SIE), TMR, and TER for the MFTJs under four resistance states, as illustrated in Fig. 4. From Fig. 4(a), one can observe that in the $P \rightarrow$ state with PC magnetic alignment, the total current is primarily contributed by the spin-up current, while the spin-down current is significantly suppressed, demonstrating an intriguing spin-filtering effect. The SIE remains 100% across the entire bias voltage range [see Fig. 4(d)]. Moreover, the total current increases with the bias voltage, then sharply decreases when the bias exceeds 0.29 V (-0.4 V), indicating the presence of a typical negative differential resistance (NDR) effect. The current peak-to-valley ratio (PVR) is crucial for applications of NDR devices. For instance, in high-frequency applications, the PVR determines the efficiency of converting d.c.-to-RF signals [39], while in multi-valued logic it defines the voltage range for transitioning to intermediate states [40]. Specifically, the current peaks at 0.29 V and reaches a minimum at 1.0 V, with a peak-to-valley difference spanning over ten orders of magnitude, resulting in an exceptionally high PVR of $9.55 \times 10^9\%$ [see Fig. 4(h)], the highest value reported to date for vertical tunnel junctions. We have also summarized a series of reported PVR values in Table SII in the Supplemental Material [38]. The current highest value, observed in the N-doped monolayer GeS system [41], is two orders of magnitude smaller than ours. As displayed in Fig. 4(b), in the APC state, the spin-filtering channel is reversed, i.e.,

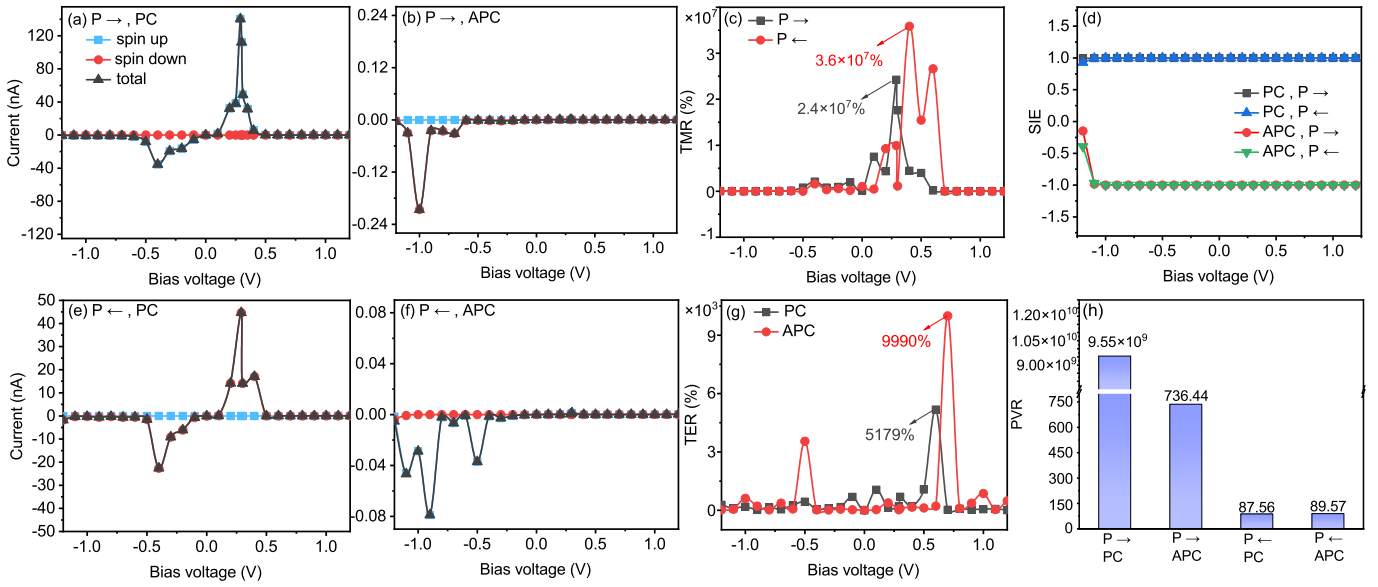


FIG. 4. The variation of the spin current [(a), (b), (e), and (f)], TMR ratio (c), TER ratio (g), and spin injection efficiency (SIE) (d) *vs* the bias voltages and the current peak-to-valley ratio (PVR) (h) in PtTe₂/CrBr₃/MnPSe₃/CrBr₃/CrBr₃(Li) MFTJs with different polarization directions and magnetic configurations.

spin-up electron transport is blocked, and the NDR effect occurs under negative bias. Comparing Figs. 4(a) and 4(b), it is clear that the current in the PC state is significantly larger than in the APC state, indicating a high TMR. For the P← state, the behavior is similar to that of the P→ state. More intriguingly, the distinction lies in the spin-filtering channel being reversed once again as depicted in Figs. 4(e) and 4(f), i.e., the PC/APC states conduct spin-down/spin-up currents, respectively. This demonstrates that the spin-filtering channel can be flexibly manipulated among the four resistance states. Furthermore, the current in the P→ state is substantially larger than in the P← state for both magnetic configurations, implying the realization of a large TER. From the I-V curves, the bias-dependent evolution of TMR and TER is derived, as shown in Figs. 4(c) and 4(g). The maximum TMR ($3.6 \times 10^7\%$) and TER (9990%) are achieved at 0.5 and 0.7 V, respectively, for the P←/APC state.

These nonequilibrium transport properties confirm that the designed vdW-MFTJs not only achieve giant TMR and TER effects but also exhibit perfect spin-filtering with switchable spin channels across a wide bias window in all four non-volatile resistance states. Additionally, they display significant PVR in the NDR effect. These findings highlight the immense potential of our MFTJs in spintronic memory applications.

Summary and Discussion.—In summary, we propose a novel vdW-MFTJ design based on a CrBr₃/MnPSe₃/CrBr₃ vertical heterostructure that exhibits genuine magnetoelectric coupling, a significant breakthrough in spintronic device engineering. This design overcomes the traditional limitations by enabling efficient spin and charge modulation through polarization switching, without the need for atomic migration

leading to symmetry breaking, as in conventional ferroelectric systems. The incorporation of asymmetric PtTe₂/alkali metal-doped/intercalated CrBr₃ electrodes leads to extraordinary tunneling magnetoresistance (TMR) and tunneling electroresistance (TER) values, exceeding $8.1 \times 10^5\%$ and 2499%, respectively, at zero bias. Under external bias, these values are dramatically enhanced, reaching up to $3.6 \times 10^7\%$ for TMR and 9990% for TER. Furthermore, the device demonstrates an exceptional negative differential resistance (NDR) effect, with a peak-to-valley ratio (PVR) of $9.55 \times 10^9\%$, the highest reported to date for vertical tunnel junctions. These outstanding properties underscore the transformative potential of vdW-MFTJs for energy-efficient electronic switching, as well as high-performance data storage and logic devices.

The observed magnetoelectric coupling arises from the intrinsic interplay between ferromagnetic CrBr₃ and antiferromagnetic MnPSe₃, amplified by the unique electronic structure at the heterointerfaces. This coupling enables precise modulation of the tunneling conductance via polarization switching, which is unattainable in conventional vdW-MFTJ designs that primarily rely on independent ferroelectric or magnetic states. Incorporating asymmetric electrodes further enhances the device performance by optimizing the spin polarization and charge transfer at the interfaces. Future work could explore alternative material combinations and stacking configurations to further improve device efficiency and expand operational versatility, paving the way for next-generation spintronic technologies.

Acknowledgement.—This work was supported by the National Natural Science Foundation of China (No. 12304148), the National Natural Science Foundation of China Regional Innovation and Development Joint Fund Key Program (No.

U24A6002), and the Shanxi Natural Science Basic Research Program (No. 202203021222219). Z.Y. was partially supported by the HZWTECH program (HZWTECH-PROP), and X.Z. by the Graduate Science and Technology Innovation Project Foundation of Shanxi Normal University (No. 2024XSY42).

* yanzhi@sxnu.edu.cn

† xuxh@sxnu.edu.cn

- [1] I. Žutić, J. Fabian, and S. D. Sarma, Spintronics: Fundamentals and applications, *Rev. Mod. Phys.* **76**, 323 (2004).
- [2] S. Wolf, D. Awschalom, R. Buhrman, J. Daughton, v. S. von Molnár, M. Roukes, A. Y. Chtchelkanova, and D. Treger, Spintronics: A Spin-Based Electronics Vision for the Future, *Science* **294**, 1488 (2001).
- [3] A. K. Geim and I. V. Grigorieva, Van der waals heterostructures, *Nature* **499**, 419 (2013).
- [4] Y. Liu, N. O. Weiss, X. Duan, H.-C. Cheng, Y. Huang, and X. Duan, Van der waals heterostructures and devices, *Nat. Rev. Mater.* **1**, 1 (2016).
- [5] K. S. Novoselov, A. Mishchenko, A. Carvalho, and A. Castro Neto, 2d materials and van der waals heterostructures, *Science* **353**, aac9439 (2016).
- [6] X. Zhai, Z. Xu, Q. Cui, Y. Zhu, H. Yang, and Y. M. Blanter, Electrically controllable van der waals antiferromagnetic spin valve, *Phys. Rev. Appl.* **16**, 014032 (2021).
- [7] Z. Yan, R. Zhang, X. Dong, S. Qi, and X. Xu, Significant tunneling magnetoresistance and excellent spin filtering effect in CrI₃-based van der Waals magnetic tunnel junctions, *Phys. Chem. Chem. Phys.* **22**, 14773 (2020).
- [8] Z. Yan, X. Jia, X. Shi, X. Dong, and X. Xu, Barrier-dependent electronic transport properties in two-dimensional MnBi₂Te₄-based van der Waals magnetic tunnel junctions, *Appl. Phys. Lett.* **118**, 223503 (2021).
- [9] H. Lin, Z. Zhang, H. Zhang, K.-T. Lin, X. Wen, Y. Liang, Y. Fu, A. K. T. Lau, T. Ma, C.-W. Qiu, *et al.*, Engineering van der waals materials for advanced metaphotonics, *Chem. Rev.* **122**, 15204 (2022).
- [10] D. L. Duong, S. J. Yun, and Y. H. Lee, van der waals layered materials: opportunities and challenges, *ACS nano* **11**, 11803 (2017).
- [11] X. Dong, X. Shen, X. Sun, Y. Bai, Z. Yan, and X. Xu, Voltage-tunable giant nonvolatile multiple-state resistance in sliding-interlayer ferroelectric *h*-BN van der Waals multiferroic tunnel junction, *Phys. Rev. B* **108**, 085427 (2023).
- [12] Z. Yan, R. Yang, C. Fang, W. Lu, and X. Xu, Giant electrode effect on tunneling magnetoresistance and electroresistance in van der Waals intrinsic multiferroic tunnel junctions using VS₂, *Phys. Rev. B* **109**, 205409 (2024).
- [13] X. Yu, X. Zhang, and J. Wang, Fully electrically controlled van der waals multiferroic tunnel junctions, *ACS nano* **17**, 25348 (2023).
- [14] Z. Yan, Z. Li, Y. Han, Z. Qiao, and X. Xu, Giant tunneling magnetoresistance and electroresistance in α -In₂Se₃-based van der Waals multiferroic tunnel junctions, *Phys. Rev. B* **105**, 075423 (2022).
- [15] Y. Feng, J. Han, K. Zhang, X. Lin, G. Gao, Q. Yang, and S. Meng, van der Waals multiferroic tunnel junctions based on sliding multiferroic layered VSi₂N₄, *Phys. Rev. B* **109**, 085433 (2024).
- [16] Y. Su, X. Li, M. Zhu, J. Zhang, L. You, and E. Y. Tsymlal, Van der waals multiferroic tunnel junctions, *Nano Lett.* **21**, 175 (2020).
- [17] A. Xie, H. Hao, C.-S. Liu, X. Zheng, L. Zhang, and Z. Zeng, Giant tunnel electroresistance in two-dimensional ferroelectric tunnel junctions constructed with a Sc₂CO₂/In₂Se₃ van der Waals ferroelectric heterostructure, *Phys. Rev. B* **107**, 115427 (2023).
- [18] Y. Zhu, B. Chi, L. Jiang, X. Guo, Y. Yan, and X. Han, Large tunneling electroresistance, tunneling magnetoresistance, and regulatable negative differential conductance in a van der waals antiferroelectric multiferroic tunnel junction, *Phys. Rev. Appl.* **20**, 034010 (2023).
- [19] X. Zhang, L. Yin, S. Zhu, R. Cheng, Y. Wen, and J. He, Spin-correlation transport and multiple resistive states in multiferroic tunnel junctions, *Phys. Rev. B* **110**, 024428 (2024).
- [20] Y. Zhang, X. Li, J. Sheng, S. Yu, J. Zhang, and Y. Su, Multilevel resistance states in van der Waals multiferroic tunnel junctions above room temperature, *Appl. Phys. Lett.* **123**, 192402 (2023).
- [21] N. A. Spaldin and R. Ramesh, Advances in magnetoelectric multiferroics, *Nat. Mater.* **18**, 203 (2019).
- [22] Y. Tokura, S. Seki, and N. Nagaosa, Multiferroics of spin origin, *Rep. Prog. Phys.* **77**, 076501 (2014).
- [23] M. Fiebig, T. Lottermoser, D. Meier, and M. Trassin, The evolution of multiferroics, *Nat. Rev. Mater.* **1**, 1 (2016).
- [24] T. Zhong, X. Li, M. Wu, and J.-M. Liu, Room-temperature multiferroicity and diversified magnetoelectric couplings in 2d materials, *Natl. Sci. Rev.* **7**, 373 (2020).
- [25] X. Liu, A. P. Pyatakov, and W. Ren, Magnetoelectric coupling in multiferroic bilayer VS₂, *Phys. Rev. Lett.* **125**, 247601 (2020).
- [26] Y. Zhao, Y. Wang, Y. Yang, J. Zhao, and X. Jiang, Realization of 2d multiferroic with strong magnetoelectric coupling by intercalation: a first-principles high-throughput prediction, *npj Comput. Mater.* **10**, 122 (2024).
- [27] W. Sun, W. Wang, D. Chen, Z. Cheng, and Y. Wang, Valence mediated tunable magnetism and electronic properties by ferroelectric polarization switching in 2D Fe₂/In₂Se₃ van der Waals heterostructures, *Nanoscale* **11**, 9931 (2019).
- [28] Y. Zhao, J.-J. Zhang, S. Yuan, and Z. Chen, Nonvolatile electrical control and heterointerface-induced half-metallicity of 2d ferromagnets, *Adv. Funct. Mater.* **29**, 1901420 (2019).
- [29] C. Huang, Y. Du, H. Wu, H. Xiang, K. Deng, and E. Kan, Prediction of intrinsic ferromagnetic ferroelectricity in a transition-metal halide monolayer, *Phys. Rev. Lett.* **120**, 147601 (2018).
- [30] J.-J. Zhang, L. Lin, Y. Zhang, M. Wu, B. I. Yakobson, and S. Dong, Type-II multiferroic Hf₂VC₂F₂ MXene monolayer with high transition temperature, *J. Am. Chem. Soc.* **140**, 9768 (2018).
- [31] N. Ding, J. Chen, S. Dong, and A. Stroppa, Ferroelectricity and ferromagnetism in a VOI₂ monolayer: Role of the Dzyaloshinskii-Moriya interaction, *Phys. Rev. B* **102**, 165129 (2020).
- [32] T. B. Prayitno and F. Ishii, First-principles study of spiral spin density waves in monolayer MnCl₂ using generalized Bloch theorem, *J. Phys. Soc. Jpn.* **88**, 104705 (2019).
- [33] H. Li and W. Zhu, Spin-driven ferroelectricity in two-dimensional magnetic heterostructures, *Nano Lett.* **23**, 10651 (2023).
- [34] W. Ding, J. Zhu, Z. Wang, Y. Gao, D. Xiao, Y. Gu, Z. Zhang, and W. Zhu, Prediction of intrinsic two-dimensional ferroelectrics in in₂se₃ and other iii2-vi3 van der waals materials, *Nat. Commun.* **8**, 14956 (2017).

- [35] R. King-Smith and D. Vanderbilt, Theory of polarization of crystalline solids, *Phys. Rev. B* **47**, 1651 (1993).
- [36] F. Wang, Y. Zhang, W. Yang, J. Zhang, H. Zhang, and X. Xu, Topological half-metallic features in alkali metal doped CrCl_3 monolayers, *Phys. Rev. B* **107**, 174405 (2023).
- [37] Y. Li, Y. Lu, P. Adelhalm, M.-M. Titirici, and Y.-S. Hu, Intercalation chemistry of graphite: alkali metal ions and beyond, *Chem. Soc. Rev.* **48**, 4655 (2019).
- [38] See Supplementary Materials at [this page](#) for the computational methods, the electronic band structures of PtTe_2 and Li-intercalated CrBr_3 , PVR values Comparison, the schematic device model and a summary table of the equilibrium transport properties of $\text{PtTe}_2/\text{CrBr}_3/\text{MnPSe}_3/\text{CrBr}_3/\text{CrBr}_3(\text{Li}$ -intercalated) MFTJ, the PDOS as and the 2D-BZ distribution of electronic transmission spectra for K/Na-doped and Li-intercalated MFTJs.
- [39] Z. Zhang, B. Zhang, Y. Wang, M. Wang, Y. Zhang, H. Li, J. Zhang, and A. Song, Toward high-peak-to-valley-ratio graphene resonant tunneling diodes, *Nano Lett.* **23**, 8132 (2023).
- [40] S. B. Jo, J. Kang, and J. H. Cho, Recent advances on multivalued logic gates: A materials perspective, *Adv. Sci.* **8**, 2004216 (2021).
- [41] C. Guo, J. Li, and T. Wang, A theoretical study on adjustment of negative differential resistance effect in monolayer gses via substitutional doping, *Phys. Status Solidi B* **260**, 2200499 (2023).